



Shear Characteristics and Failure Mode of Hard Brittle Marl with Parallel Discontinuous Structural Plane

Zhiming Yin^{1,2,3} · Xinrong Liu^{1,2,3} · Zhongping Yang^{1,2,3} · Yuanwen Jiang^{1,2,3} · Yalong Zhao^{1,2,3} · Shiqi Li^{1,2,3}

Received: 12 February 2020 / Accepted: 25 May 2020 / Published online: 8 June 2020
© King Fahd University of Petroleum & Minerals 2020

Abstract

Engineering practice shows that the failure of rock bridges between structural planes which makes the discontinuous structural plane evolve into a continuous sliding fracture plane leads the instability of many slopes. In order to further understand the shear failure mechanism of rock mass with discontinuous structural plane, the direct shear tests under different normal pressures were carried out on the hard brittle limestone samples with different structural plane dip angles. The test results show that the fracture surface of rock bridge is mainly tensile failure, while both sides of the fracture surface are mainly shear failure. Both two flanks and the middle fracture surface show that both ends of the fracture surface are mainly shear failure, while the middle of the fracture surface is mainly tensile failure. When σ is large and α is small, the rock is mainly shear failure. When σ is large and α is large, or σ is small and α is small, the rock is mainly tension-shear mixed failure. When σ is small and α is large, the rock is mainly tensile failure. The failure mode of the sample may vary with the change of the structural plane inclination and normal stress. But overall speaking, it can be summarized as five typical failure modes that are STS–STS–STS, STS–T–STS, S–STS–S, S–S–S and T–T–T. The peak shear stress of the sample increases with the increase in normal stress, and decreases first and then increases with the increase in the dip angle of the structural plane. When $\alpha = 0^\circ$, the peak shear stress is the largest; when $\alpha = 45^\circ$, the peak shear stress is the smallest. When α is small, the shear strength of the sample is mainly affected by the inclination angle θ of the rock bridge. When α is large, the shear strength of the sample is mainly affected by the length L of the rock bridge.

Keywords Parallel discontinuous structural plane · Dip angle · Normal stress · Shear properties · Failure modes

1 Introduction

A large number of discontinuous interface, such as fractures, faults and joints, exist in the rock mass of slope, which play an important role in the stability of slope [1–5]. In natural rocks, preexisting flaws usually appear in sets or groups

with similar orientations and characteristics [6, 7]. Engineering practice shows that the failure of rock bridges between structural planes, which makes the discontinuous structural plane evolve into a continuous sliding fracture plane, leads the instability of many slopes [8–13], such as the fracture of Aishihik river bank slope in Canada [10] (Fig. 1a), the

✉ Xinrong Liu
liuxrong@126.com

✉ Zhongping Yang
yang-zhp@163.com

Zhiming Yin
yzm001129@163.com

Yuanwen Jiang
571379270@qq.com

Yalong Zhao
1793626627@qq.com

Shiqi Li
451860580@qq.com

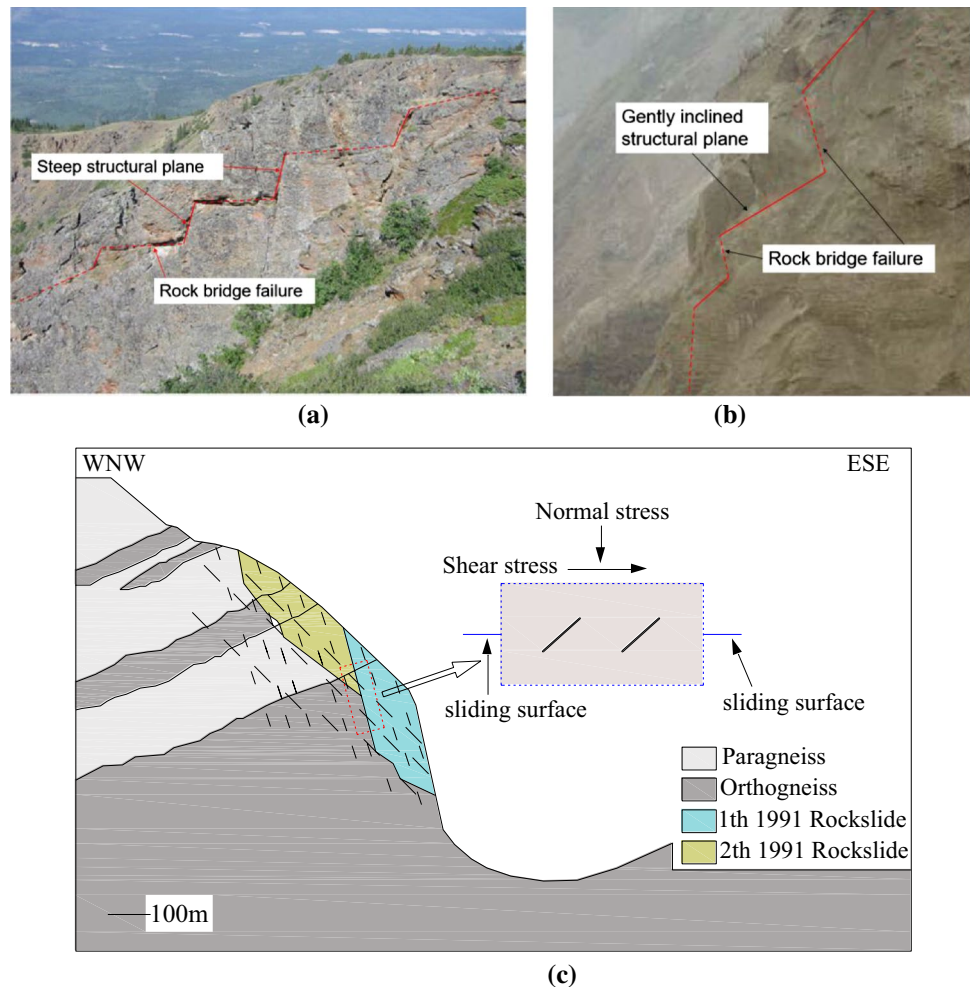
¹ School of Civil Engineering, Chongqing University, Chongqing 400045, China

² Key Laboratory of New Technology for Construction of Cities in Mountain Area (Chongqing University), Ministry of Education, Chongqing 400045, China

³ National Joint Engineering Research Center for Prevention and Control of Environmental Geological Hazards in the TGR Area Chongqing University, Chongqing 400045, China



Fig. 1 Examples of landslide along discontinuity structural plane (a the Aishihik River landslide; b the step-path failure in the reservoir slopes of the Xiaowan hydroelectric station, China; c the 1991 Randa rockslide) [10, 11, 13]



sliding slope of Xiaowan Hydropower Station in China [11] (Fig. 1b), and the 1991 Randa rockslide [13] (Fig. 1c). In the construction of highway, tunnel and other engineering activities, the excavation of slope toe and the underground mining unloading may lead to the connection of the structural plane rock bridge in the upper high steep slope and finally break. In general, the shear strength of the slope along the discontinuous discontinuity is controlled by the contact surface and the rock bridge between the discontinuities with different shear mechanisms [14]. Therefore, in addition to the discontinuity itself, the rock bridge between discontinuities plays a very important role to the shear strength of the composite failure surface. It is still necessary to improve the understanding of the shear failure mechanism of the rock bridge between discontinuities.

A large number of studies had been carried out on the expansion of intermittent fracture rock bridges under uniaxial or biaxial compression [15–19]. However, in the high and steep slope rock mass, the failure of jointed rock mass is very common when the minimum principal stress is tensile stress. This kind of stress state is difficult to appear in the

common uniaxial or triaxial test. However, the direct shear test can simulate the stress characteristics of jointed rock mass in which the minimum principal stress may be tensile stress. In addition, the direct shear test can fully consider the influence of the geometry and position of the intermittent joint rock mass, the shear strength parameters of the structural plane and the rock bridge under different normal stresses on the propagation and connection of the intermittent joint [20, 21].

As early as 1969, direct shear tests under different normal stresses were carried out on the gypsum samples containing two coplanar joints by Lajtai [20]. The results showed that the initial crack direction of intermittent jointed rock mass was not consistent with the shear direction, and the normal stress had a great impact on the failure mechanism of rock bridge. Three failure modes, tension failure, shear failure and compression failure, were defined. The envelope of shear strength and shear strength criterion was also established. Zhou [22] carried out the direct shear tests on the rock-like materials with non-through jointed rock mass. According to the characteristics of acoustic emission in shear process, the

process of propagation and transfixion of jointed rock mass was divided into four stages: precrack stage, micro-crack stage, instability stage and friction stage. Bai et al. [23] carried out direct shear tests on the non-through jointed rock mass made of the mixture of sand, gypsum and water. It was found that the normal stress, joint connectivity and arrangement mode had an important influence on the expansion of the non-through jointed rock mass. Through experiments, Liu et al. [24] found that the extension and transfixion of discontinuous jointed rock mass can be divided into three modes: tension failure, tension-shear composite failure and shear failure. And based on the theory of Lajtai rock bridge, considering the horizontal compressive stress of shear unit, the strength criteria are derived, respectively. The direct shear tests on non-coplanar and non-through joints were carried out by Savilahti and Stephansson [25]. It was found that for the joint specimen with two joints parallel to the shear direction, the failure starts from the near end of the two joints, and extends and finally penetrates in the direction close to the vertical direction of the joint surface. In addition, Ghazvinian et al. [26] and Sarfarazi et al. [27] studied the shear fracture behavior of rock-like samples with coplanar intermittent cracks of horizontal and vertical separation. However, the influence of the dip angle of structural plane on the fracture mechanism of rock bridge was not considered in the above studies. Zhang [13] used shear box experiments and rock failure process simulation methods to study the effects of parallel intermittent fissure density on shear failure of rock-like specimen rock bridges. Gehle [28] carried out direct shear tests on gypsum samples with five joints of different angles parallel to each other. It was found that according to the strength change of non-through joints, the process from the beginning of loading to the maximum displacement can be divided into three stages: joint extension through, rock bridge rotation and joint plane sliding. And many failure modes were found, including tension failure in the initial crack, shear failure in the through failure and failure caused by rock bridge rotation.

Generally speaking, there were many studies on the shear failure of intermittent jointed rock mass, but the influence of the dip angle of structural plane (the angle between structural plane and shear direction) on the shear failure of rock bridge was seldom considered. With different dip angles of structural planes, the stress state and stress concentration of rock bridge are quite different, which leads to great differences in shear failure characteristics of rock bridge. On the other hand, the existed research mainly focuses on the shear test of gypsum or gypsum sand mixture rock-like materials, while the mechanical properties of gypsum and other rock-like materials are quite different from the real rock. Gehle [28] considered the influence of the dip angle of the structural plane, but used gypsum like rock materials. Therefore, in this study, the direct shear tests under different normal

pressures were carried out on the hard brittle limestone samples with different structural plane dip angles.

2 Direct Shear Test

2.1 Sample Design

The rock selected in the test was a hard brittle marl with an average uniaxial compressive strength of 92 MPa and a uniaxial tensile strength of 5.6 MPa. All rock samples were from the same parent rock and were cut in parallel and vertical bedding directions (shear direction was consistent with bedding direction). Considering the length and width requirements of the specification [29] and the size limit of the thickness of the rock plate cut by the water jet cutter, test samples were processed into a long square body with the size of 100 mm × 60 mm × 40 mm. The length of the structural plane was fixed at 20 mm, the spacing was fixed at 40 mm, the width of the joint was controlled within 2 mm, and the center point of the structural plane was fixed on the shear plane of the sample. The dip angle α of the structural plane of the sample was considered to be horizontal, gentle, inclined, steep and vertical, which are, respectively, 0°, 20°, 45°, 65° and 90°. The geometric structure and loading mode of the sample are shown in Fig. 2.

2.2 Sample Processing

The processing of specimens was divided into four steps that are rough block cutting by rock cutter, surface initial leveling by grinding wheel, surface fine leveling by rock sample grinder and structural surface cutting by high-speed water cutter. Dimension deviation was controlled within 0.2 mm, and verticality deviation was controlled within 0.2°. The sample preparation process is shown in Fig. 3.

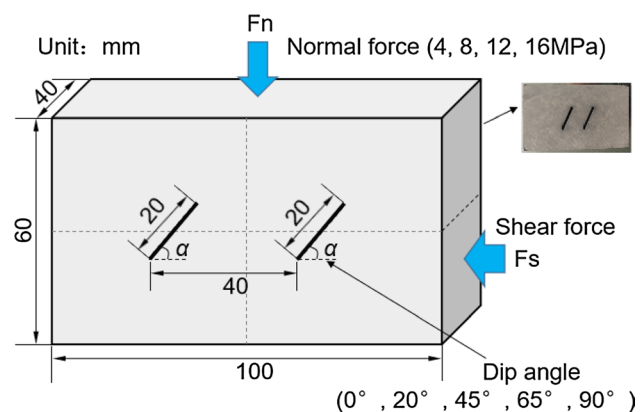


Fig. 2 Geometrical dimension and loading mode of specimens

Fig. 3 Rock samples processing flow

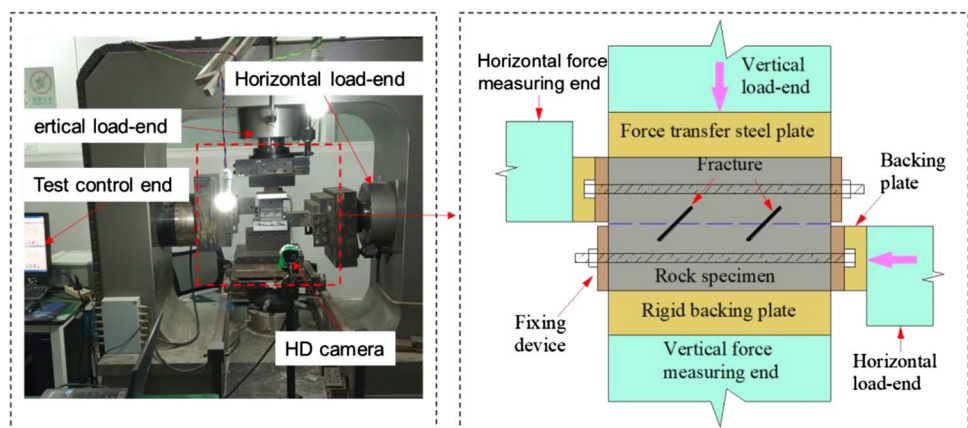


2.3 Test Equipment and Loading Scheme

In this test, two influencing factors of structural plane inclination and normal stress were considered. The structural plane inclination was considered to be 0° , 20° , 45° , 65° and 90° , and the normal stress was considered to be 4 MPa, 8 MPa, 12 MPa and 16 MPa (as shown in Fig. 2). The test was carried out on WDAJ-600 electro-hydraulic servo rock shear rheological testing machine (as shown in Fig. 4). Firstly, the axial force of the specimen was loaded

to the target value, and the loading mode was stress control mode, and the loading rate was 0.1 kN/s. After the axial force loading was stable, kept the axial force unchanged, and then applied the tangential force until the tensile or shear through failure of the specimen occurs. The loading mode was displacement control mode, and the loading rate was 0.1 mm/min. When installing the specimen, make sure that the specimen and the shear head were placed in the center, so as to prevent bias during the shearing process, resulting in the error of the test results. In order to reduce the influence

Fig. 4 Test system and sample layout



of the end effect on the test results, a proper amount of butter was applied to the upper and lower end faces of the test piece before the test, to reduce the friction constraint between the test piece and the rigid pressure plate and the stress concentration during the loading process. At the same time, during the loading process, high-definition camera was used to record the whole process of shear failure of the specimen. Three repeated tests were carried out for each working condition to ensure that at least two test results are similar, and a typical one was selected for analysis.

3 Test Results and Discussion

3.1 Characteristics of Shear Stress–Displacement Curves

The shear stress–displacement curves of specimens with different structural plane inclinations under different normal stresses are shown in Fig. 5. Figure 5 shows that the shear stress–displacement curves of parallel intermittent joint rock mass had obvious segmented characteristics, which can be divided into four deformation and failure stages: compaction stage of structural plane, quasi-linear deformation stage, unstable fracture development stage before peak and residual fracture stage after peak. The

shear stress–displacement curves can well reflect the shear failure characteristics. Taking the shear stress–displacement curve of specimen with structural plane inclination of 45° under normal stress 4 MPa as an example, the failure stages were described, respectively, as follows (as shown in Fig. 6):

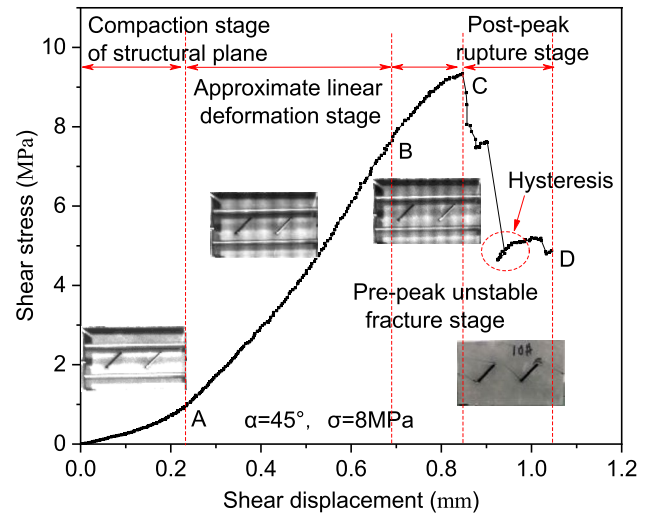
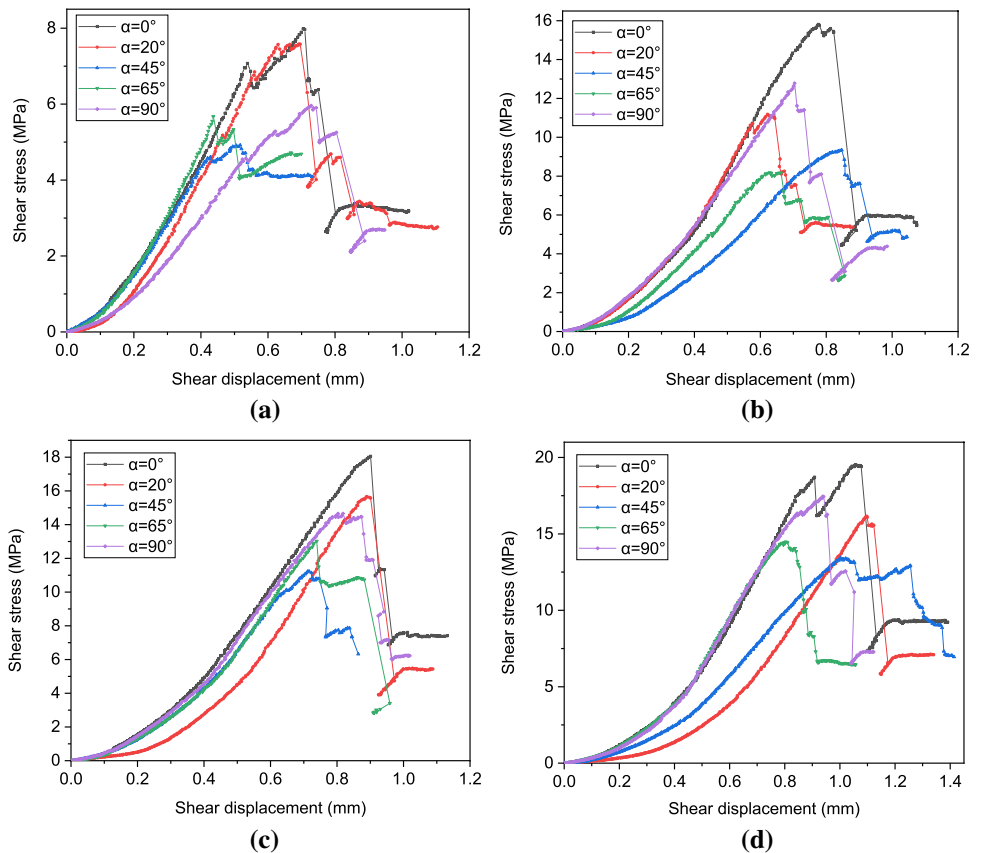


Fig. 6 Failure stage division of shear stress–displacement curve

Fig. 5 Shear stress–displacement curves of specimens with different crack dips (a $\sigma=4$ MPa; b $\sigma=8$ MPa; c $\sigma=12$ MPa; d $\sigma=16$ MPa)



1. Compaction stage of structural plane (OA in Fig. 6): at the initial stage of loading, the shear stress increased relatively slowly, and the curve was obviously upward concave. In this stage, the structural plane and internal pores of the specimen were compacted, which leads to the closure of the prefabricated structural plane and primary microcracks.
2. Quasi-linear deformation stage (AB in Fig. 6): In this stage, the slope of the curve was large and the shear stress increased rapidly. Different from the shear stress–displacement curve of complete rock, it was not completely linear deformation. In addition to the elastic shear deformation of rock, there was also existing small shear deformation of the prefabricated structural plane. And with the increase in shear stress, local cracks often occurred at the non-end parts of the structural plane, which was called the initial crack here. The secondary cracks propagated and rapidly steadied. Due to the generation of secondary cracks, the energy at the joint tip was released, and the stress was transferred to the adjacent rock units. Macroscopically, the shear strength was not lost due to local secondary cracks, but continues to increase.
3. Unstable fracture development stage before peak (BC in Fig. 6): After the initial fracture in the former stage, when the strain energy continues to accumulate to a certain extent, the continuous microbrittle fracture of the rock bridge occurred again. In this stage, unstable fracture began to occur, the shear stress growth trend slowed down, and the curve was slightly downward concave. The slight “snap” sound caused by brittle fracture of the sample can be heard from time to time. With the increase in shear stress, the fracture propagation and breakthrough path with the minimum energy consumption were found, a macro fracture surface was formed, and meanwhile, the shear stress reached its peak. There were three kinds of curves in this stage: (1) Before the peak stress, the curve was generally slightly concave downward and no obvious stress drop, such as the curve of $\alpha=0^\circ$ in Fig. 5b, which reflects the continuous crack growth process. (2) The linear growth of the previous stage was basically maintained before the peak, the downward concave section lasted for a short time, and there was also no obvious stress drop before the peak, such as the curve of $\alpha=20^\circ$ in Fig. 5d, which shows the process of crack sudden growth and penetration. (3) There was obvious stress drop before the peak, such as the curve of $\alpha=20^\circ$ in Fig. 5b, indicating that the direction or position of crack propagation changed, or the failure mode changed in the propagation path.
4. Residual fracture stage after peak (CD in Fig. 6): In this stage, the shear stress decreased sharply, and its decline process was multi-step. Each sharp decline was due

to the development of local fracture of the specimen. When the peak strength was reached, the internal energy of the specimen was released suddenly, accompanied by a sharp crackle, which shows a sudden stress drop on the curve. After that, under the action of a certain positive pressure, the fracture surface was compacted. Due to the friction action and the bite action of fracture fragments, the shear resistance gradually increased and finally became stable, and may form a curve hysteresis loop. With the continuous application of shear action, the specimen cannot shear sliding along the macrostructural plane when the angle of fracture surface or normal stress is large, resulting in gnawing failure once again and stress drop.

3.2 Analysis of section characteristics and failure modes of specimens

Based on the high-definition camera, the crack propagation process of the rock sample can be clearly observed and the fracture properties of the propagation crack can be preliminarily determined. The failure modes and section morphology of all the specimens are shown in Fig. 7. By observing the shape of the fracture surface, it was found that the shear failure was often accompanied by white shear and extrusion scratches, shear debris and shear fracture zone, while the tensile fracture section was often rough and gray and without white rock powder, as shown in Fig. 8. Based on this feature, the section features and failure modes of specimens with different dip angles under different normal stresses were analyzed.

Due to the difference of processing accuracy between rock sample and structural surface, the section characteristics and failure modes of some samples were relatively complex, but on the whole, there were relatively obvious rules. Figure 7 shows that the fracture surface of the rock between the structural planes ran through along the direction of the rock bridge, and the direction of the fracture surface of the rock on both sides was roughly parallel to the direction of the rock bridge. There were less shear scratches on the fracture surface of the rock bridge, mainly tensile failure, while there were many shear scratches on the fracture surface of both sides, mainly shear failure. Both two flanks and the middle fracture surface showed that there were more scratches on both ends of the fracture surface, mainly shear failure, while there were less scratches on the middle of the fracture surface, mainly tensile failure. The section shape and failure mode of the sample may vary with the change of the structural plane inclination and normal stress. Overall speaking, it can be summarized as five typical failure modes, as shown in Fig. 9 (*S* for shear failure and *T* for tension failure).

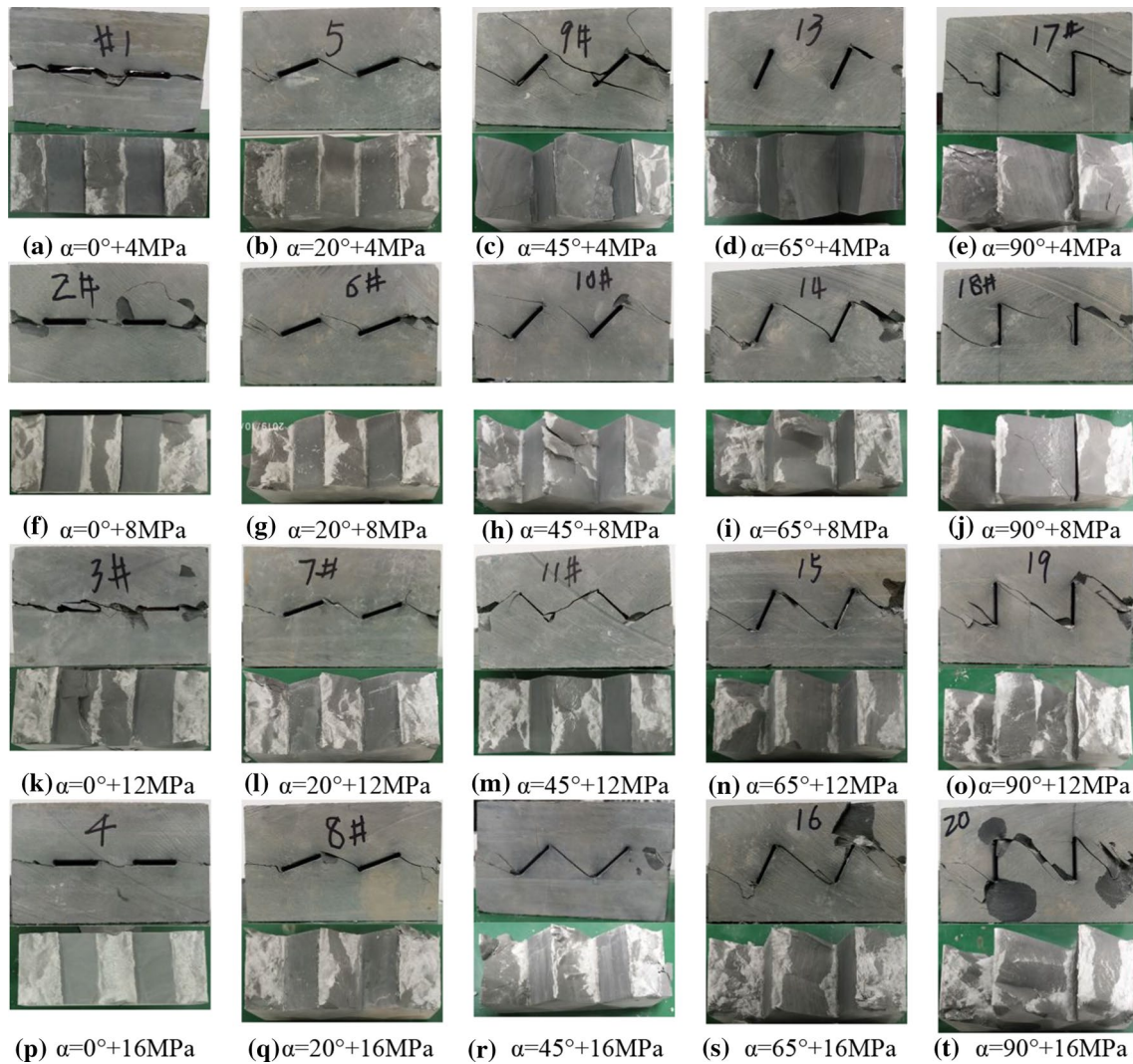


Fig. 7 Section characteristics and failure modes

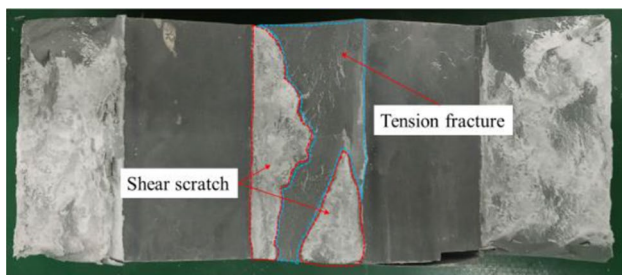


Fig. 8 Characteristics of fracture surface

In order to further analyze the influence of the structural plane inclination and normal stress level on the failure characteristics and failure mode of the specimen, the ratio of the shear scratch area of the fracture surface of the upper half of the specimen to the total fracture surface area (expressed

by ζ) was calculated. And the relationship curves between ζ and the structural plane dip angle (α) and normal stress (σ) were obtained as shown in Figs. 10 and 11, respectively.

(1) Influence of structural plane inclination

Figure 10 shows that the curve of the relationship between ζ and α under different normal stresses was basically the same shape and can be divided into region I (0° – 45°) and region II (45° – 90°) with the boundary of $\alpha = 45^\circ$. When $\alpha \in$ I, ζ decreased obviously with the increase in α , but when $\alpha \in$ II, ζ changed less obviously with the increase in α . It was shown that $\alpha \in$ I was the transition region of the failure mode from shear failure to tension-shear mixed failure, while $\alpha \in$ II was the stable region of tension-shear mixed failure and tension failure. From Figs. 7 and 10, it can be seen that only the case of $\alpha = 65^\circ$ and $\sigma = 4$ MPa was close to pure tensile failure, and only the case of $\alpha = 0^\circ$ and $\sigma = 16$ MPa was near pure shear failure, and the others were mixed tensile-shear

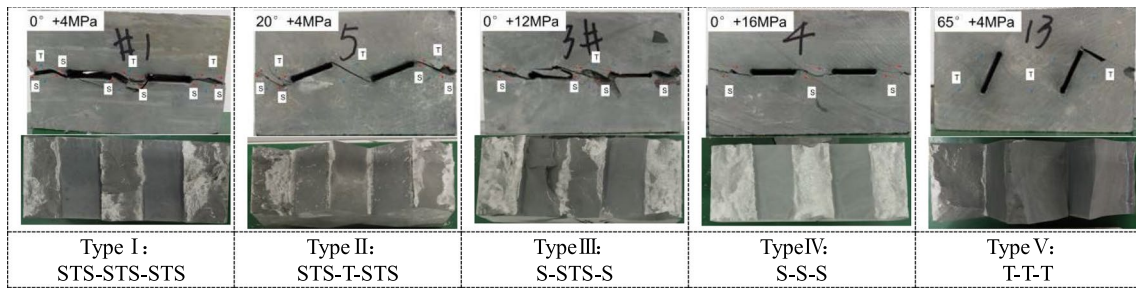


Fig. 9 Five typical failure modes

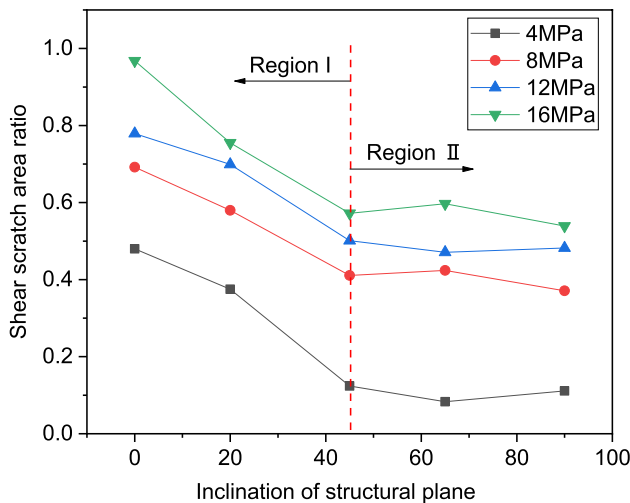


Fig. 10 Relationship between scratch area ratio and inclination of structural surface for different values of σ

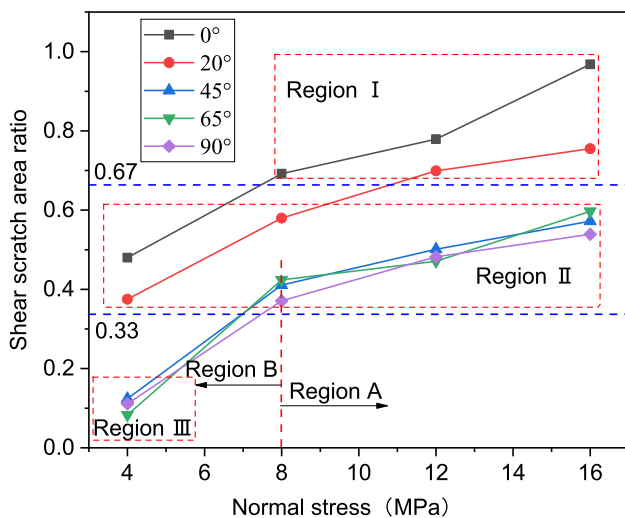


Fig. 11 Relationship between scratch area ratio and normal stress for different values of α

failure modes, indicating that the conditions of pure tensile failure and pure shear failure that occur were harsh. It can be considered that pure tensile failure can occur only when $\alpha \in \text{II}$ and σ are very small, and pure shear failure can occur only when $\alpha \in \text{I}$ and σ are very large. From the above analysis, it can be inferred that when σ is very small, with the increase in α , the failure mode of the sample changes from tension-shear mixed failure (a–c in Fig. 7) to tension-shear mixed failure (d in Fig. 7), and then back to tension-shear mixed failure (e in Fig. 7). When σ is very large, with the increase in α , the failure mode of the sample changes from shear failure (p in Fig. 7) to tension-shear mixed failure [(d) failure (q), (r), (s) and (t) in Fig. 7]. In other cases, no matter what value α is, only tension-shear mixed failure occurs.

(2) The influence of normal stress

From Fig. 11, we can see that ζ increases with σ at all structural plane angles, indicating that with the increase in normal stress, the proportion of shear failure area on the failure section of the specimen increases, and the specimen changes from tension-shear mixed failure to shear failure. In addition, when $\alpha \in \text{II}$, the curve can also be divided into region A (4–8 MPa) and region B (8–16 MPa) with $\sigma = 8$ MPa as the boundary. When $\sigma \in \text{B}$, ζ increases rapidly with the increase in σ , while when $\alpha \in \text{A}$, the increase in ζ slows down with the increase in σ . It shows that when the dip angle of the structural plane is large, and the normal stress is low, with the increase in the normal stress, the specimen changes rapidly from the tension-shear mixed failure dominated by tensile failure to the tension-shear mixed failure dominated by shear failure.

According to the definition of ζ , $\zeta \in (0,1)$. ζ was mainly related to the failure mode of the sample. It was assumed that the larger the ζ was, the more obvious the shear failure characteristic of the specimen was, and the smaller ζ was, the more obvious the tensile failure characteristic of the specimen was. Taking 0.33 and 0.67 as boundary points, the value range of ζ is divided into three equal span areas I, II and III. According to Fig. 11 we knew that:

When σ is large and α is small, $\zeta \in (0.67, 1)$, such as region I in Fig. 11, the specimen is mainly shear failure. When σ is large and α is large, or σ is small and α is small, $\zeta \in (0.33, 0.67)$, such as region II in Fig. 11, the specimen is mainly tension-shear mixed failure. When σ is small and α is large, $\zeta \in (0, 0.33)$, such as region I in Fig. 11, the specimen is mainly tensile failure.

3.3 Peak Shear Strength Analysis

According to the above analysis, the failure modes of the specimen are greatly affected by the inclination of the structural plane and the normal stress. The failure modes of the specimen directly affect the strength characteristics of the specimen. Figure 12 shows the relationship curve between peak shear stress and structural plane inclination angle α under different normal stresses of the sample. It can be seen that under the same structural plane inclination, the peak shear stress of the sample increases with the increase in normal stress. And under the same normal stress, the peak shear stress decreases first and then increases with the increase in the dip angle of the structural plane. When $\alpha = 0^\circ$, the peak shear stress is the largest; when $\alpha = 45^\circ$, the peak shear stress is the smallest.

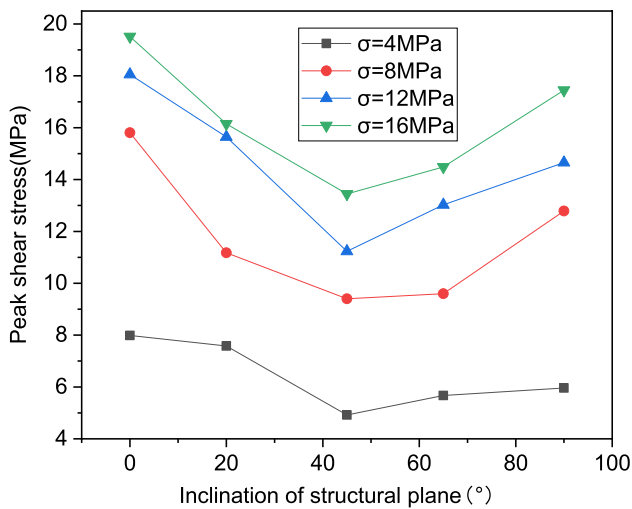
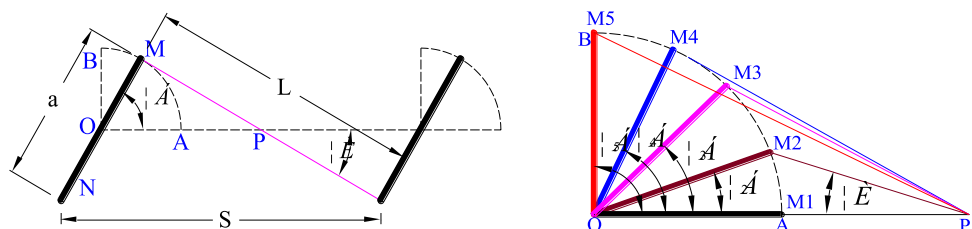


Fig. 12 Peak shear stress versus the structural plane inclination α for different values of σ

Fig. 13 Geometric relationship between rock bridge and structural plane



According to the above analysis of the section characteristics of the specimen, it can be seen that the change rule of the area ratio ζ of the shear scratch with α is not completely consistent with the change rule of the peak shear stress with α , which shows that the rule of describing the fracture characteristics and the peak shear stress characteristics of the specimen only by the angle of the structural plane is not clear. Therefore, the failure mode and strength characteristics of rock bridge are summarized in terms of rock bridge inclination (θ) and rock bridge length (L). According to the geometric relationship (such as Fig. 13), the dip angle (θ) and length (L) of rock bridge can be expressed by the dip angle (α) and spacing (S) of structural plane according to the formula (1) and (2):

$$\theta = \arctan\left(\frac{\sin \alpha}{\frac{S}{a} - \cos \alpha}\right) \tag{1}$$

$$L = a\sqrt{1 + \left(\frac{S}{a}\right)^2 - 2\frac{S}{a}\cos \alpha} \tag{2}$$

In this study, fixed $a = 20$ mm, $s = 40$ mm, from (1) and (2) we can get:

$$\theta = \arctan\left(\frac{\sin \alpha}{2 - \cos \alpha}\right) \tag{3}$$

$$L = 20\sqrt{5 - 4\cos \alpha} \tag{4}$$

According to Eqs. (3) and (4), the relationship curves of θ , L and α are shown in Figs. 14 and 15, respectively.

According to Fig. 14, when $\alpha \in (0^\circ, 60^\circ)$, θ monotonically increases with α , and the increasing rate is smaller and smaller. When $\alpha \in (60^\circ, 90^\circ)$, θ monotonically decreases with α . When $\alpha = 60^\circ$, the maximum value of θ is 30° . If only the change of θ is considered, and the change of L is not considered, according to the test results, it can be inferred that the peak shear stress has a negative correlation with θ . $\Delta\gamma_1$ is the average change of θ per 10° in the range of $\alpha \in (0^\circ, 36.7^\circ)$, which is equal to 7.2° . $\Delta\gamma_2$ is the average change of θ per 10° in the range of $\alpha \in (36.7^\circ, 90^\circ)$, which is only 0.6° . It shows that when α is small, the change of θ has great influence on the peak

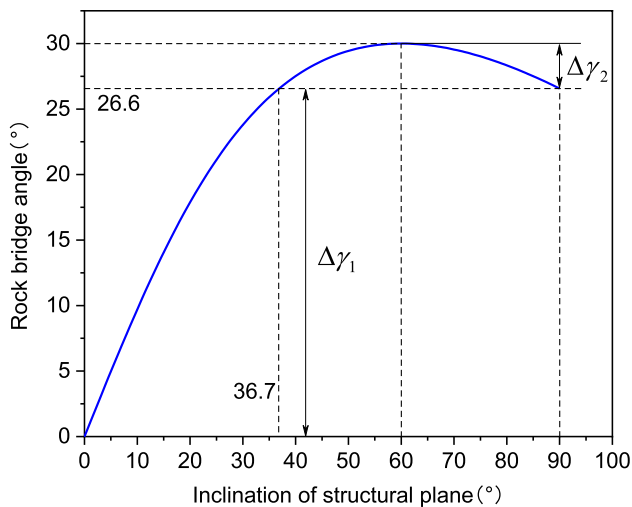


Fig. 14 Relationship between rock bridge angle θ and inclination of structural plane α

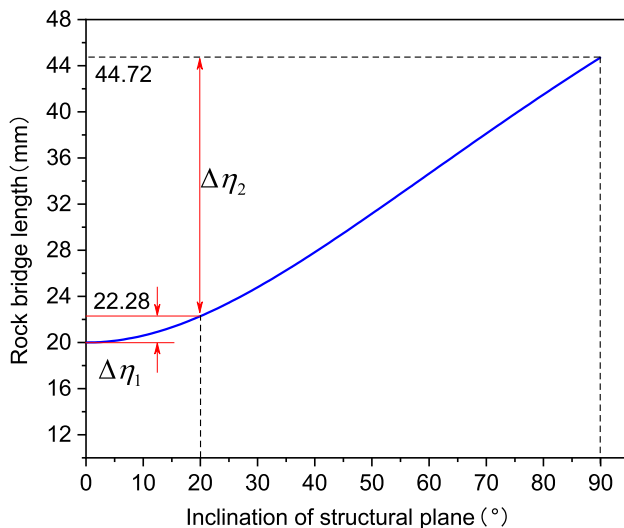


Fig. 15 Relationship between rock bridge length L and inclination of structural plane α

shear stress, while when α is large, the change of θ has little influence on the peak shear stress.

Figure 15 shows that the length L of rock bridge increases monotonically with the increase in α , and the increase rate is slow when α is small. If only the change of rock bridge length is considered, the change of rock bridge angle θ is not considered, as we all know, the shear strength of the sample is positively related to the length of the rock bridge. $\Delta\eta_1$ is the average change of L per 10° in the range of $\alpha \in (0^\circ, 20^\circ)$, which is equal to 3.2 mm. $\Delta\eta_2$ is the average change of L per 10° in the range of $\alpha \in (20^\circ, 90^\circ)$, which is only 1.1 mm. It shows that when α is small, the change of L has little effect on the peak shear stress,

while when α is large, the change of L has great effect on the peak shear stress.

Now, considering both the change of dip angle and length of rock bridge, the change characteristics of peak shear stress are analyzed. When $\alpha \in (0^\circ, 60^\circ)$, θ and L increase with the increase in α . The increase in θ makes the peak shear stress decreasing and the decreasing rate of peak shear stress decreasing. The increase in L makes the peak shear stress increasing and the increasing rate of peak shear stress increasing. Therefore, the combined action of θ and L makes the peak shear stress decreasing first and then increasing. From Fig. 12, it can be seen that the peak shear stress is the smallest when $\alpha = 45^\circ$. When α is small, the shear strength of the sample is mainly affected by the inclination angle θ of the rock bridge. When α is large, the shear strength of the sample is mainly affected by the length L of the rock bridge.

The failure characteristics of the specimen are mainly affected by the inclination of the rock bridge. When α is small ($\alpha \in (0^\circ, 45^\circ)$), the inclination angle θ of the rock bridge increases greatly, which results in a significant decrease in the shear friction area ζ ratio of the fracture section. When α is large ($\alpha \in (45^\circ, 90^\circ)$), the change angle of the inclination angle θ of the rock bridge is very small, so the area ζ of the shear scratch on the failure section does not change significantly.

4 Conclusion

The shear stress–displacement curves of parallel intermittent joint rock mass had obvious segmented characteristics, which can be divided into four deformation and failure stages: compaction stage of structural plane, quasi-linear deformation stage, unstable fracture development stage before peak and residual fracture stage after peak. The biggest difference from complete rock mass was that in compaction stage of structural plane, the shear stress increases relatively slowly because of the closure of the prefabricated structural plane, and multi-step stress drops failure in residual fracture stage after peak.

The fracture surface of the rock between the structural plane runs through along the direction of the rock bridge, and the direction of the fracture surface of the rock on both sides is roughly parallel to the direction of the rock bridge. There are less shear scratches on the fracture surface of the rock bridge, mainly tensile failure. There are many shear scratches on both sides of the fracture surface, mainly shear failure. Both two flanks and the middle fracture surface show that there are more scratches on both ends of the fracture surface, mainly shear failure, while there are less scratches on the middle of the fracture surface, mainly tensile failure. The section shape and failure mode of the sample may vary with the change of the structural plane inclination and

normal stress. Overall speaking, it can be summarized as five typical failure modes: STS–STS–STS, STS–T–STS, S–STS–S, S–S–S and T–T–T.

ζ is mainly related to the failure mode of the sample. When σ is large and α is small, $\zeta \in (0.67, 1)$, the specimen is mainly shear failure. When σ is large and α is large, or σ is small and α is small, $\zeta \in (0.33, 0.67)$, the specimen is mainly tension-shear mixed failure. When σ is small and α is large, $\zeta \in (0, 0.33)$, the specimen is mainly tensile failure.

Under the same structural plane inclination, the peak shear stress of the sample increases with the increase in normal stress. And under the same normal stress, the peak shear stress decreases first and then increases with the increase in the structural plane inclination. When $\alpha = 0^\circ$, the peak shear stress is the largest; when $\alpha = 45^\circ$, the peak shear stress is the smallest.

When $\alpha \in (0^\circ, 60^\circ)$, θ and L increase with the increase in α . The increase in θ makes the peak shear stress decreasing and the decreasing rate of peak shear stress decreasing. The increase in L makes the peak shear stress increasing and the increasing rate of peak shear stress increasing. The combined action of θ and L makes the peak shear stress decreasing first and then increasing. The peak shear stress is the smallest when $\alpha = 45^\circ$. When α is small, the shear strength of the sample is mainly affected by the inclination angle θ of the rock bridge. When α is large, the shear strength of the sample is mainly affected by the length L of the rock bridge.

Acknowledgements The authors acknowledge the financial support from the National Key R&D Program of China (Grant No. 2018YFC1504802) and the Fundamental Research Funds for the Central Universities (Project NO. 2019CDXYTM0032) and the National Natural Science Foundation of China (Grant No. 41972266). We also thank Bin Xu, a graduate student, for his efforts in conducting the laboratory tests.

References

- Hoek, E.: Strength of jointed rock masses. *Geotechnique* **33**(3), 187–223 (1983)
- Guo, S.F.; Qi, S.W.: Numerical study on progressive failure of hard rock samples with an unfilled undulate joint. *Eng. Geol.* **193**, 173–182 (2015)
- Zhou, X.P.; Zhang, J.Z.; Qian, Q.H.; et al.: Experimental investigation of progressive cracking processes in granite under uniaxial loading using digital imaging and AE techniques. *J. Struct. Geol.* **126**, 129–145 (2019)
- Zhu, T.T.; Huang, D.: Experimental investigation of the shear mechanical behavior of sandstone under unloading normal stress. *Int. J. Rock Mech. Min. Sci.* **114**, 186–194 (2019)
- Zhao, Z.L.; Jing, H.W.; Shi, X.S.; et al.: Experimental and numerical study on mechanical and fracture behavior of rock-like specimens containing pre-existing holes flaws. *Eur. J. Environ. Civil Eng.* (2019). <https://doi.org/10.1080/19648189.2019.1657961>
- Gratchev, I.; Dong, H.K.; Chong, K.Y.: Strength of rock-like specimens with preexisting cracks of different length and width. *Rock Mech. Rock Eng.* **49**, 4491–4496 (2016)
- Zhang, J.Z.; Zhou, X.P.; Zhou, L.S.; Berto, F.: Progressive failure of brittle rocks with non-isometric flaws: Insights from acousto-optic-mechanical (AOM) data. *Fatigue Fract. Eng. Mater. Struct.* **42**(8), 1787–1802 (2019)
- Terzaghi, K.; Hon. M.A.S.C.E.; M.I.C.E: Stability of steep slopes on hard unweathered rock. *Geotechnique* **12**, 251–270 (1962)
- Eberhardt, E.; Stead, D.; Coggan, J.S.: Numerical analysis of initiation and progressive failure in natural rock slopes—the 1991 Randa rockslide. *Int. J. Rock Mech. Min. Sci.* **41**(7), 69–87 (2004)
- Brideau, M.-A.; Yan, M.; Stead, D.: The role of tectonic damage and brittle rock fracture in the development of large rock slope failures. *Geomorphology* **103**(1), 30–49 (2009)
- Huang, D.; Cen, D.F.; Ma, G.W.; et al.: Step-path failure of rock slopes with intermittent joints. *Landslides* **12**(5), 911–926 (2015)
- Huang, R.Q.; Qi, S.W.: Engineering geology: ten years review and prospect. *J. Eng. Geol. Chin.* **25**(2), 257–276 (2017)
- Zhang, K.; Chen, Y.L.; Fan, W.C.; et al.: Influence of intermittent artificial crack density on shear fracturing and fractal behavior of rock bridges: experimental and numerical studies. *Rock Mech. Rock Eng.* (4):1–16 (2019)
- Liu, D.Y.; Ye, X.M.; Zhu, F.: The ultimate strength evaluation of rock mass containing intermittent joints. *J. Chongqing Jianzhu Univ. Chin.* **19**(2), 21–30 (1997)
- Wong, R.H.C.; Chau, K.T.: Crack coalescence in a rock-like material containing two cracks. *Int. J. Rock Mech. Min. Sci.* **35**(2), 147–164 (1998)
- Sagong, M.; Bobet, A.: Coalescence of multiple flaws in a rock-model material in uniaxial compression. *Int. J. Rock Mech. Min. Sci.* **39**, 229–241 (2002)
- Yang, S.Q.; Dai, Y.H.; Han, L.J.; et al.: Experimental study on mechanical behavior of brittle marble samples containing different flaws under uniaxial compression. *Eng. Fract. Mech.* **76**(12), 1833–1845 (2009)
- Wong, L.N.; Einstein, H.H.: Crack coalescence in molded gypsum and Carrara marble: part I. Macroscopic observations and interpretation. *Rock Mech. Rock Eng.* **42**(3), 475–511 (2009)
- Zhang, J.Z.; Zhou, X.P.; Zhu, J.Y.; et al.: Quasi-static fracturing in double-flawed specimens under uniaxial loading: the role of strain rate. *Int. J. Fract.* **211**(2), 1–28 (2018)
- Lajtai, E.Z.: Shear strength of weakness planes in rock. *Int. J. Rock Mech. Min. Sci. Geomech. Abstr.* **6**(5), 499–515 (1969)
- Liu, Y.M.; Xia, C.C.: Advances in research of rock masses containing discontinuous joints in direct shear test. *Rock Soil Mech. Chin.* **28**(08), 198–203 (2007)
- Zhou, Q.L.; Liu, G.F.: Compression shear fracture of brittle materials. *J. Hydraul. Eng. Chin.* **7**, 63–67 (1982)
- Bai, S.W.; Ren, W.Z.; Feng, D.X.; et al.: Research on the strength behavior of rock containing coplanar close intermittent joints by direct shear test. *Rock Soil Mech. Chin.* **20**(2), 10–16 (1999)
- Liu, Y.M.: Study on Failure Models and Strength of Rockmass Containing Discontinuous Joints in Direct Shear. Tongji University, Shanghai (2007)
- Savilabti, T.; Nordlund, E.; Tephansson, O.: Shear box testing and modeling of joint bridge [A]. In: *Rock joints: Proceedings of the International Symposium on Rock Joints*. A.A. Balkema: Rotterdam (1990)
- Ghazvinian, A.; Sarfarazi, V.; Schubert, W.; et al.: A study of the failure mechanism of planar non-persistent open joints using PFC2D. *Rock Mech. Rock Eng.* **45**(5), 677–693 (2012)
- Sarfarazi, V.; Ghazvinian, A.; Schubert, W.; et al.: Numerical simulation of the process of fracture of echelon rock joints. *Rock Mech. Rock Eng.* **47**(4), 1355–1371 (2014)
- Gehle, C.; Kutter, H.K.: Breakage and shear behavior of intermittent rockjoints. *Int. J. Rock Mech. Min. Sci.* **40**, 687–700 (2003)
- National Standards Compilation Group of People's Republic of China. Standard for tests method of engineering rock masses (GB/T 50266-2013). China Planning Press, Beijing (in Chinese) (2013)

